Chapter 11
Microclimate Models for a Sustainable and Liveable Urban Planning

Guglielmina Mutani and Francesco Fiermonte

Abstract Globally, the 54% of the world's population reside in urban areas, and in 2050 the projections are of 66%. Then the sustainability and livability of urban spaces are rising the attention of the scientific community. Particularly, in this work, the microclimate of outdoor spaces is investigated considering the different outdoor air temperatures registered by various weather stations in the city of Turin (Italy). The air temperature variations were correlated with the characteristics of the different spaces as the built urban morphology, the solar exposure of urban spaces and the albedo coefficients of outdoor surfaces. Finally, with a multiple linear regression analysis, the air temperatures have been correlated with the urban variables to obtain a model for the prediction of the average monthly temperature in the city of Turin. This model will be used to understand the different microclimates in Turin but also to evaluate the most influential urban variables on the air temperature. Moreover, the resulted model could help urban planners to predict the microclimate in new districts as a function of the urban form and of the outdoor materials chosen.

Keywords Microclimate • Urban heat island • Urban planning • Air temperature model

11.1 Introduction

Nowadays, people live more in urban areas (54% in 2014) than in rural areas, and this trend is still growing with a prevision of 66% in 2050. The most urbanized regions include Northern America and Europe (respectively, with 82 and 73% of

G. Mutani (✉)
Department of Energy, Politecnico di Torino,
Corso Duca degli Abruzzi, 24, 10129 Turin, Italy
e-mail: guglielmina.mutani@polito.it

F. Fiermonte
Interuniversity Department of Regional and Urban Studies and Planning,
Politecnico di Torino, Viale Mattioli, 39, 10125 Turin, Italy
e-mail: francesco.fiermonte@polito.it

R. Ingaramo, A. Voghera (eds.), *Topics and Methods for Urban and Landscape Design*, Urban and Landscape Perspectives 19,
DOI 10.1007/978-3-319-51535-9_11

people living in urban areas), and all regions are expected to urbanize further over the coming decades (United Nations 2014).

Then, the control of the microclimate of urban environment became a very important matter as it can contribute to a better livability of the cities with an improved use of the outdoor spaces. In big cities, this phenomenon is strongly linked to the urban heat island (UHI), and these aspects are treated in the first part of this work as state-of-art and literature review.

The second part of the work is dedicated to the evaluation of various factors influencing the air temperature and its variations in the urban context of Turin. Turin is one of the most populous cities in the northern part of Italy with an interesting various territory with parks, rivers, a historical centre, suburban areas and industrial zones.

The aim of this work is to elaborate a model for the prediction of air temperature as a function of urban variables, solar exposition and the characteristics of outdoor surfaces. Particular attention will be paid to factors influencing or closely related to the urban heat island, as already underlined in the previous works.

Different tools have been used to evaluate the microclimate at urban scale. ESRI ArcGIS 10.3 has been utilized to calculate the urban characteristics with a detailed representation of the built environment, starting from the Technical Map of the Metropolitan City of Turin. For the evaluation of the characteristics of outdoor urban surfaces, several images coming from the Aster satellite have been processed. Finally, five different zones in Turin with a weather station inside have been selected to elaborate a model to predict the air temperature as a function of the urban form, the solar exposure and the albedo coefficient of outdoor surfaces. The resulting model can be useful in the design phase in order to plan a more sustainable urban development or to control air temperature variation in the urban space. The model can also help in understanding how temperature changes depend on urban planning variables, as the presence of rivers and green surfaces, giving indications on the interventions that can mitigate the overheating effect.

Some of the results show the urban heat island effect with lower temperatures near the parks and the riversides and higher temperature in the high-density centre and industrial zones. These results will be further investigated on a larger zone around Turin considering more weather stations, other satellite images as the Landsat ones and additional indicators, for example, the normalized vegetation index (NDVI).

The analysis conducted in this work starts from previous researches on the influence of different materials used for outdoor urban spaces on the microclimate of urban environments (Mazzotta and Mutani 2015), on the evaluation of the urban form of buildings' heritage and its influence on urban microclimate and heating energy consumptions of residential buildings (Delmastro et al. 2015a, b) and on the urban heat island effect in Turin (Mutani 2016; Mutani et al. 2016).

11.2 State of the Art and Literature Review

The urban overheating problem is a matter of fundamental importance that all the developed and the developing countries are studying to mitigate its effects. For big cities, this issue is strongly linked to the thermal phenomenon called urban heat island (UHI).

Starting from the 1970s, thanks especially to the availability of data, tools and techniques were improved, and new algorithms and computational models have been formulated to understand and analyse more deeply the heat island phenomenon. The first studies on this phenomenon were based on the acquisition of satellite images (i.e. Landsat) to calculate the land surface temperatures (LSTs) and to observe how this parameter changes according to the different types of urban surfaces.

Several studies (Aniello et al. 1995; Iino and Hoyano 1996; Jusuf et al. 2007) analyse the relationship between land use and land cover (LULC) to understand how human activities can influence the intensity of the heat islands. The first results show that the heat island is mostly concentrated in urban areas, while the phenomenon is not observed in the surrounding rural areas (Li et al. 2009; Unger et al. 2010; Onischi et al. 2010): this is why the temperature measured in urban context is higher than in the peripheral zones.

Later studies begin to take into account different variables and factors that may affect the intensity of UHI as the relationship between land use and type of coverage (LULC), the normalized vegetation index (NDVI) and the land temperature surface (LST). All these factors were calculated by elaborating satellite images, such as Landsat and ASTER, through the use of specialized software capable in the localizing information, such as geographic information system (GIS) (Weng et al. 2004; Onischi et al. 2010; Li et al. 2011; Zhang et al. 2012, 2013; Xu et al. 2013; Effat and Hassan 2014; Kong et al. 2014; Shahidan et al. 2015; Fernàndez et al. 2015).

Together with these studies, a very important aspect to be taken into account is the variations of microclimate and UHI with the urban morphology. Depending on the different types of buildings and urban forms, the urban heat island has different intensities. Some researchers have investigated the changes of UHI with the urban characteristics, i.e. the urban density, the urban form and height of buildings (Aniello et al. 1995; Iino and Hoyano 1996; Weng et al. 2004; Unger et al. 2010; Li et al. 2011; Houet and Pigeon 2011; Zhang et al. 2012; Schwartz et al. 2012; Merbitz et al. 2012; Li et al. 2012; Chun B and Guldmann 2014; Ivajnsic et al. 2014; Allegrini et al. 2014; Kong et al. 2014; Sailor 2014; Dabaieh et al. 2015). These parameters are also used to describe the urban canyon phenomenon, characterized by high buildings facing on the same street. In this condition, the solar radiation is almost completely absorbed by urban surfaces, and the air stagnates, with an increase of air temperatures and, consequently, the urban overheating. As well as with these parameters, also the characteristics of materials, as the albedo coefficient, should be considered. This parameter is an intrinsic characteristic of the materials and represents the property of a material to reflect incident solar irradiation. In fact, a material such as asphalt, with very low of albedo value, tends to store and absorb all the incident solar irradiation, reaching higher surface temperatures than clay materials that absorb less heat and have less high surface temperatures.

Many studies evaluate algorithms to calculate albedo coefficients using satellite images on different electromagnetic bands (Li et al. 2009; Stathopoulou and Cartalis 2009; Mallick et al. 2013; Kolokotroni et al. 2014; Santamouris 2014a ; Salata et al.

2015; Thophilou and Serghiedes 2015; Qin 2015; Coseo and Larsen 2015, Pisello 2015).

Nowadays, to investigate the UHI effect, the microclimate and the outside air temperature variations, the urban morphology, the properties of the open space materials (with the albedo coefficient) and the surfaces' temperature have been analysed (Effat and Hassan 2014; Balogun et al. 2014; Zhang et al. 2014; Pisello and Cotana 2014, 2015; Santamouris 2014b; Fernàndez et al. 2015; Yang et al. 2015; Touchaei and Wang 2015; Debbage and Shepherd 2015; Kaloustian and Diab 2015; Fernàndez et al. 2015; Berger et al. 2015. Santamouris et al. 2015; Quan et al. 2015; Coseo and Larsen 2015; Mirzaei 2015; Raghavan et al. 2015; Peron et al. 2015; Yang et al. 2015).

While almost all of the analysed documents are proposing to investigate the heat islands and their effect on urban temperatures, other studies are focusing, instead, on the influence of the overheating on thermal comfort and on energy consumptions (Balogun et al. 2014; Zhang et al. 2014; Santamouris 2014a, b; Pisello 2015; Gracik et al. 2015; Santamouris et al. 2015; Misni 2015; Liu et al. 2015). These studies focus more on the heating than the cooling energy uses; obviously, the outside temperatures strongly influence the energy consumptions for space heating and cooling, but also the electrical consumptions are influenced by the outside microclimate. These researches evaluate solutions to reduce the heat island effect, air pollution, energy consumptions and costs. The main ideas concern the use of mitigation techniques to reduce the air temperature in urban areas. One method is to replace the traditional roofs with "cold roofs" made from tiles or slates in clay. In fact, these surfaces guarantee higher albedo coefficients able to reflect the solar irradiation with lower temperatures (Pisello and Cotana 2014, 2015; Dabaieh et al. 2015).

Other studies are focused, instead, on the use of the green on buildings' roofs or facades or on parking structures; through evapotranspiration, external temperature is lower (Zhang et al. 2014; Kong et al. 2014; Fernàndez et al. 2015; Qin 2015; Raghavan et al. 2015).

It was also analysed the so-called cold asphalt, the last generation of asphalts with very-high albedo values, able to reflect solar irradiation and keep lower temperatures than traditional bituminous asphalt (Carnielo and Zinzi 2014; Qin 2015).

In almost the cited studies, the relationships between the outside air temperatures and some of the parameters mentioned above are investigated. Some of them provided also a model or an algorithm, to be used in the design phase, in order to create a more sustainable urban planning (Iino and Hoyano 1996; Unger et al. 2010; Yeo et al. 2013; Chun and Guldmann 2014; Feng et al. 2014; Ivajnsic et al. 2014; Allegrini et al. 2014; Zhang et al. 2014; Kolokotroni et al. 2014; Fernàndez et al. 2015; Quan et al. 2015; Morris et al. 2015).

In this work all the parameters characterizing the urban morphology, the solar exposure and the albedo coefficients will be analysed in relation to air temperature variation to define an algorithm for the evaluation and prediction of the microclimate in Turin.

11.3 Case Study: Turin

Turin is the fourth most populous Italian town in the North-West part of Italy with a particular territory characterized by surrounding mountains and hills, by many rivers and parks and an elegant built context.

Turin is called "the city of four rivers" because it is localized in a plain surrounded by Stura di Lanzo, Sangone and Po rivers with also the Dora Riparia flowing close to its historical centre. Its territory is also surrounded by the Alpine mountains, also connecting the city with France. Moreover, Turin is the Italian city with more public green with about 21.1 m^2 of green per capita and about 160,000 trees along the streets and in the parks.

The climate is continental temperate with cold-dry winters and hot-humid summers, and, as the majority of urbanized territories, Turin is characterized by the UHI phenomenon with significantly higher temperatures than in the rural and hilly areas around the city. Considering the weather stations inside the town, there are differences on the monthly average air temperature principally due to the buildings' density, the presence of industrial zones and the proximity of parks and rivers.

From the 1990s, the summers have registered a significant warming, especially from the year 2000; the maximum air temperature was recorded in the hot summer 2003 with a peak of 39.7 °C in August 11.

In Fig. 11.1, the monthly average air temperatures registered by the ARPA weather stations in Turin from June 2005 to June 2015 are represented (ARPA is the Regional Agency for the Protection of the Environment of Piedmont Region).

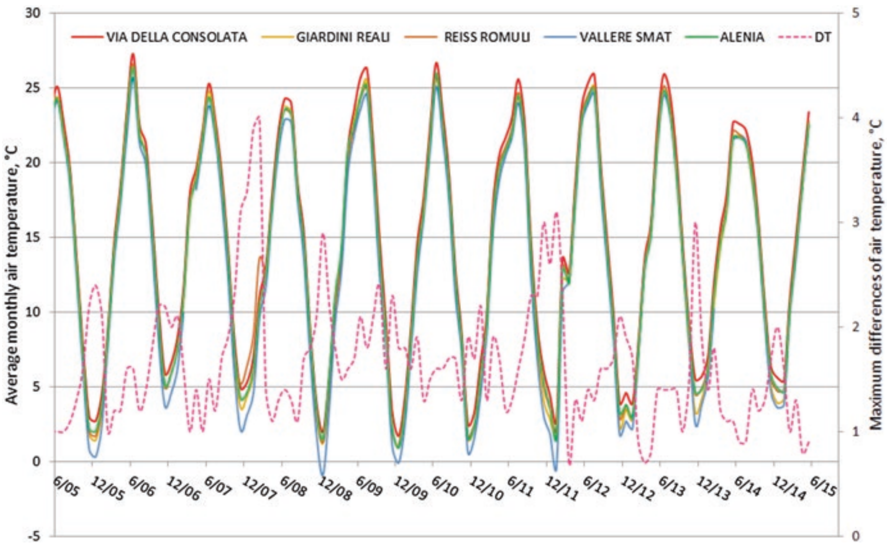

Fig. 11.1 Average monthly air temperatures registered in five ARPA weather stations in Turin

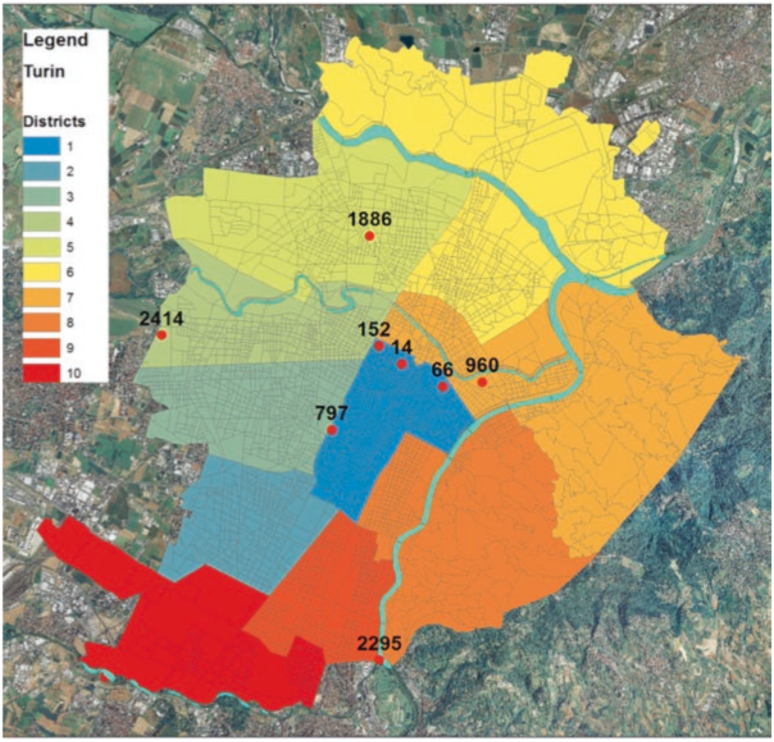

Fig. 11.2 The eight weather stations in the city of Turin with the indication of the relative census sections and the ten districts (Source: author's elaboration)

As it is possible to note, the temperature differences vary from 2 to 4 °C during the cold months and from 0 to 2 °C during the hot months. Much more differences are registered considering the minimum air temperature values with differences up to 9 °C from the different weather stations.

In Turin, in the last 10 years, the average value of heating degree days (*HDD*), for the heating seasons, is of about 2350 HDD with a standard deviation of about 200 HDD. The coldest area is Vallere (with parks and the Po river) and the warmest is via della Consolata (with a high buildings' density).

In Figs. 11.2 and 11.3, the position of eight weather stations in the city of Turin is represented. Particularly, some weather stations are localized in the high buildings' density zones, others in suburban zones and two of them in the parks; one of these, Vallere in the census section n. 2295, is near the Po river. The four rivers Po, Dora Riparia, Stura di Lanzo and Sangone can be recognized, respectively, in the east side near the hill, through Turin centre, in the northern part and in proximity to Turin's southern boundary.

In this work the causes of air temperature differences in the city of Turin are analysed considering also the different urban contexts in the census parcels in which the weather stations are localized.

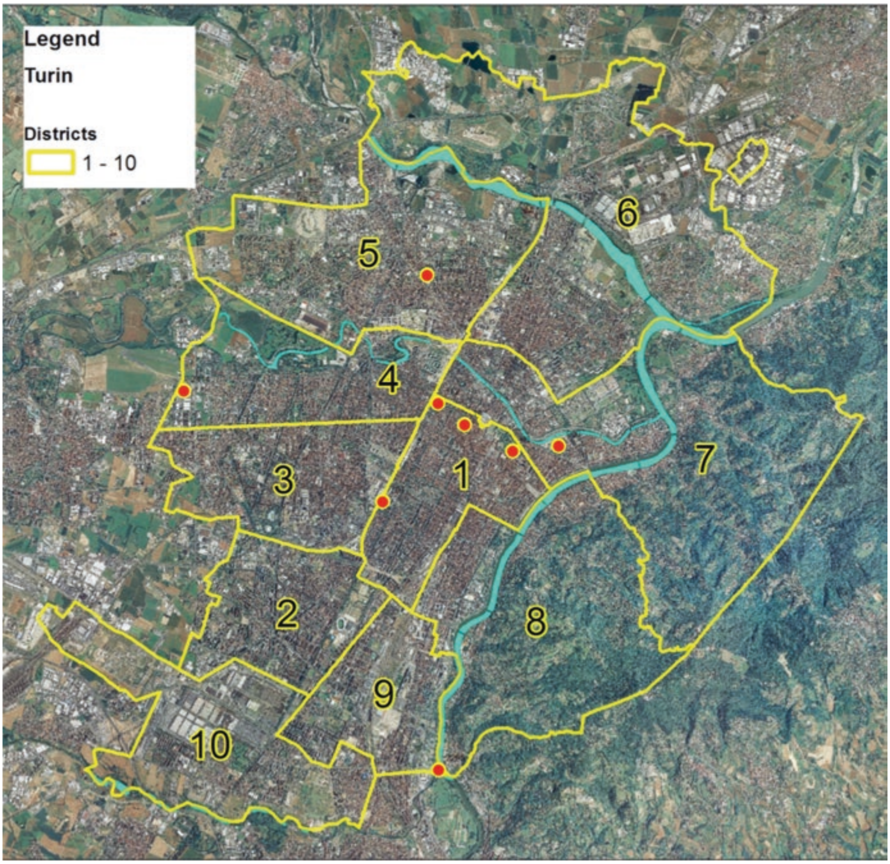

Fig. 11.3 The eight weather stations in the city of Turin with the representation of the urban context in which they are localized and the relative district (Source: author's elaboration)

11.4 Instruments and Methods

The aim of this work is to analyse how the built environment can influence the microclimate of different urban contexts. This analysis is focused on the census parcels, in which the weather stations of the city of Turin are localized (Fig. 11.2).

The variables analysed to characterize the built environment can be summarized in an urban morphology factor (*U*), a "solar exposure" (*P*) factor and the albedo coefficient (*A*) of outdoor materials.

The urban morphology characteristics (*U*) represent the contribution of the form of the built environment affecting the outdoor air temperature variation. The urban morphology is influenced mainly by the following variables: the buildings' density (*BD*) and the average buildings' distance (*W*) or the buildings' coverage ratio (*BCR*) and the aspect ratio (height to buildings' distance, *H*/*W*).

The urban morphology factor (U) can be expressed by

$$U = BD / W = BCR \cdot H / W [-]. \tag{11.1}$$

The solar exposure (P) is the function of the ratio between the height of the building and the height of the surroundings (H/H_{avg}), the main buildings' orientation (MBO) and the main orientation of the streets (MOS)

$$P = H / H_{avg} \cdot MBO \cdot MOS [-]. \tag{11.2}$$

The optimal orientation for buildings and streets for solar exposure is the east-west direction; then different values have been assigned to the *MBO* and *MOS* as shown in Fig. 11.4.

For the calculation of the albedo coefficient A, the correlations founded in literature have been used (Liang 2000 and Liang et al. 2002) using ASTER images. The sensor Advanced Spaceborne Thermal Emission and Reflection Radiometer (ASTER) is a satellite remote sensor providing high-resolution images of the earth in 14 different wavelengths on the electromagnetic spectrum.

ASTER images, in the Tagged Image File Format (TIFF), contain information relating to the radiance measured according to the wavelength of the sensor and expressed in the form of digital numbers (DN). To convert the DN in spectral radiance and top of atmosphere (TOA) radiance, specific correlations and coefficients can be used (Ghulam 2009; Banerjee et al. 2014).

From the spectral radiance and TOA radiance, it is possible to apply the equations of Liang, in order to calculate the albedo coefficient for all the wavelength bands of ASTER sensor. In particular, in this work, the data have been proceeded according to the Liang correlations for near-infrared ASTER albedo coefficient, using the satellite images relating to VNIR 1–2–3 bands (visible and near infrared) and 4–5–6–7–8–9 SWIR (shortwave infrared). The images of the ASTER sensor were provided by CSI (Consortium for Information System of Piedmont Region) and are related to the acquisition of July 22nd, 2004.

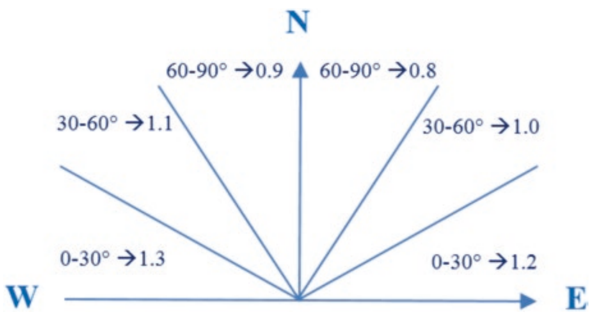

Fig. 11.4 Values for the main orientation of streets and buildings (MOS, MBO) (Source: author's elaboration)

Finally, each single urban variable is analysed with its average value considering its relative census section. For each census section, a global value G is then defined:

$$G(U, P, A)[-] \tag{11.3}$$

considering the variables of "urban morphology factor" (U), "solar exposure" (P) factor and albedo coefficient (A).

In this work, the urban variables of five different census sections are compared considering the average monthly air temperatures registered by the weather stations in Turin.

11.5 Results and Discussion

The city of Turin is localized in the Po Valley, and it is surrounded by beautiful mountains and hills. Turin is an important nineteenth-century city with historical buildings, beautiful squares and outdoor spaces but also industrial zones.

The area of the census sections in the city of Turin is not uniform due to districts with very large census sections as the hilly area (districts 7 and 8) and the industrial areas (districts 6 and 10) as shown in Figs. 11.2 and 11.3. The average size of the sections of the Turin census is about 35,000 m^2, with 17% of roads and 19% of built area (which becomes 23% if only the blocks of buildings are considered). Among this analysis, the census sections that are closest to these average values are the weather stations of Reiss Romoli (census section n.1886 in the northern area of Turin) and Buon Pastore (census section n.152 that is now no longer active). The characteristics of the census sections analysed with the weather stations are reported in Table 11.1.

Table 11.1 Characteristics of the census sections with the analysed weather stations

Turin's weather station	Weather station ARPA number	Census section number	Census section area (m^2)	Building area (m^2)	Building volume (m^3)	Streets area (m^2)	Blocks of buildings area (m^2)
via della Consolata	3447	14	8132	3529	59,535	2599	5533
Giardini Reali	446	66	79,070	565	6234	29,965	49,105
Reiss Romoli	3869	1886	52,790	16,866	210,907	9106	43,683
Vallere	249	2295	316,919	42,913	316,778	70,213	246,706
Alenia	4294	2414	405,096	146,901	1,686,958	39,184	365,912
Buon Pastore	153	152	52,756	13,963	165,401	8566	44,190
Italgas	145	960	130,323	23,165	172,352	40,245	90,079
Politecnico di Turin	–	773	183,878	41,534	418,532	97,665	86,214
Turin (average)		**1–3850**	**33,773**	**6426**	**83,008**	**5704**	**28,069**

In Figs. 11.5 and 11.6, the values of the "urban morphology factor" (*U*) and "solar exposure" (*P*) factor are represented for each census section of the city of Turin. From Fig. 11.5, the high buildings' density zone in the centre, the hilly part of the city in the south-east side and the industrial zones in the northern and southern parts can be recognized.

From Fig. 11.6, the solar exposure factor (*P*) is represented. The differences depend also by the orientation and the dimension of the census sections.

In Figs. 11.7 and 11.8, the albedo coefficient (*A*) is represented, respectively, with punctual values and average values for the census parcels. From Fig. 11.7, natural elements as the rivers and the hilly zone can be noticed; also the industrial roofs in the northern and southern part of the city can be noticed.

Finally, in Fig. 11.8, the average value of the albedo coefficient was calculated for each census parcel. Higher values can be noticed in the central zone of the city and along the rivers; instead, lower values of albedo coefficient characterize the industrial zones with lighter colour roofs.

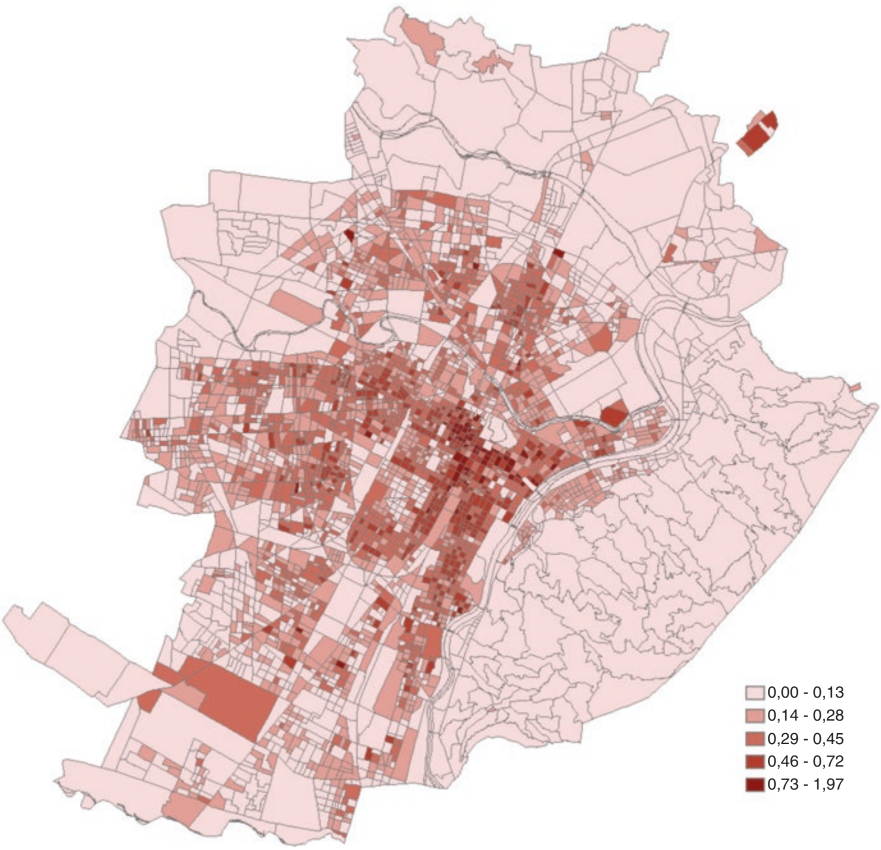

Fig. 11.5 The urban morphology factor U for the census sections of the city of Turin

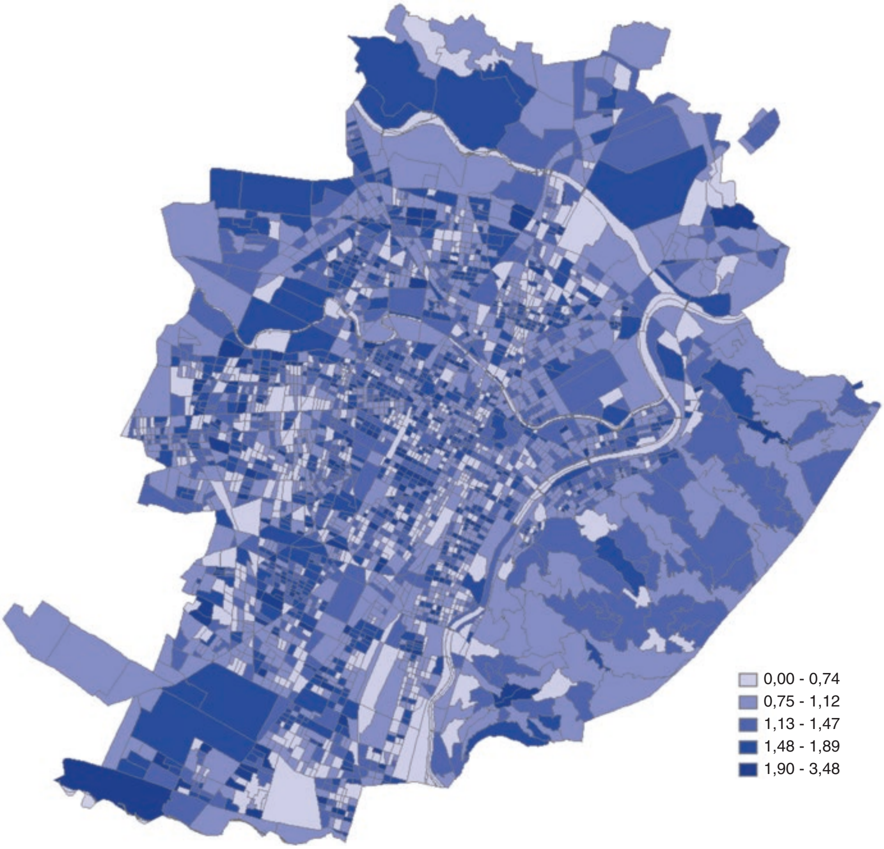

Fig. 11.6 The solar exposure factor P for the census sections of the city of Turin

In Table 11.2, the main characteristics about the urban form (*U*), solar exposure (*P*) and albedo coefficient (*A*) of the census parcels analysed are reported (with the ARPA weather stations). In particular, the high buildings' density (*BD*) values can be noticed for the areas with the weather stations of via della Consolata, Reiss Romoli, Alenia, Buon Pastore and Politecnico di Torino; lower values of *BD* can be observed in Giardini Reali and Vallere which are localized in parks and Vallere also near the Po river; finally, the Italgas weather station is in an ex-industrial zone.

The aspect ratio (*H/W*) is higher also for the high-density central zone, and, about the orientation of streets (*MOS*) and buildings (*MBO*), the main orientation is south, south-west and south-east.

Starting from these urban data, the aim of this work is to derive a model for the outdoor air temperature considering the average monthly data. This model could allow understanding, at the first design-planning phase, the effect of the materials, the geometric buildings' forms, the characteristics of outdoor spaces and the solar exposition, on the performance of air temperatures; the model could be used as a

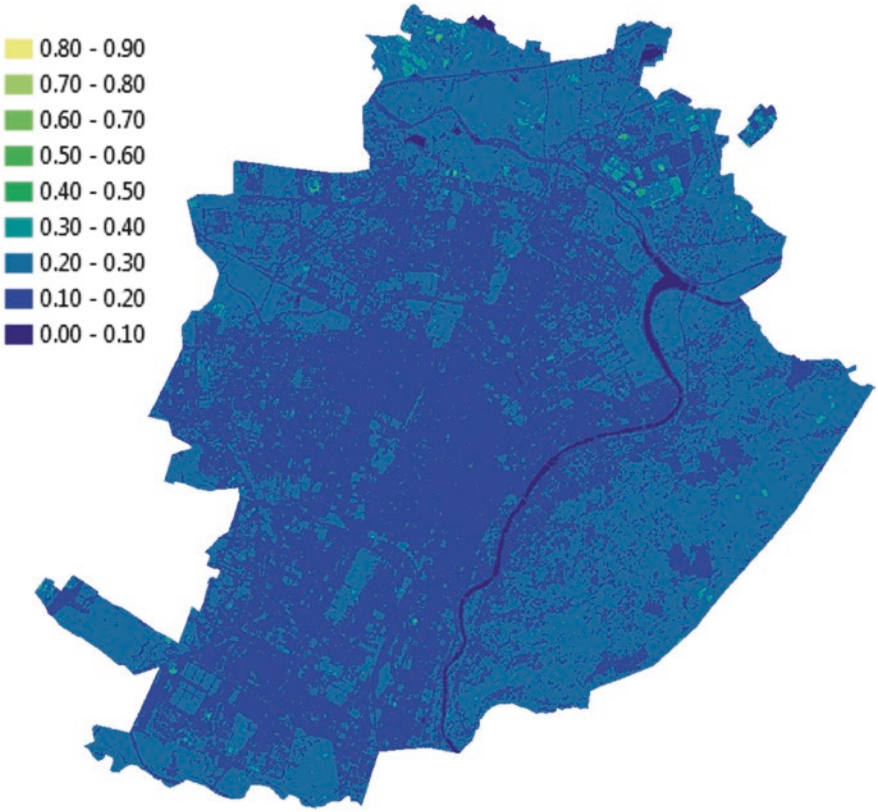

Fig. 11.7 The albedo coefficient A in Turin (obtained from ASTER images of July 22nd, 2004)

tool to improve environmental sustainability and urban liveability in urban planning.

For a good design tool, the model should evaluate the average monthly air temperature for a prediction in all seasons, especially during wintertime and summertime.

A multiple linear regression analysis correlates the urban variables $G(U, P, A)$ to the average air temperatures considering also a typical monthly air temperature behaviour for Turin (ΔT_m)

$$\begin{aligned} T_{air} &= f(GUPA) = f(\Delta T_m, BCR, H/W, MOS, H/H_{\text{aver}}, MBO, A) \\ &= (\alpha_1 \cdot \Delta T_m) + (\alpha_2 \cdot BCR) + (\alpha_3 \cdot H/W) + (\alpha_4 \cdot MOS) + (\alpha_5 \cdot H/H_{\text{aver}}) + (\alpha_6 \cdot MBO) \\ &\quad + (\alpha_7 \cdot A)[°C]. \end{aligned} \tag{11.4}$$

where ΔT_m is the monthly variation of the air temperatures considering weather data from 2006 to 2014 averaged on the actual functioning five ARPA weather stations in Turin: via della Consolata, Giardini Reali, Reiss Romoli, Vallere and Alenia.

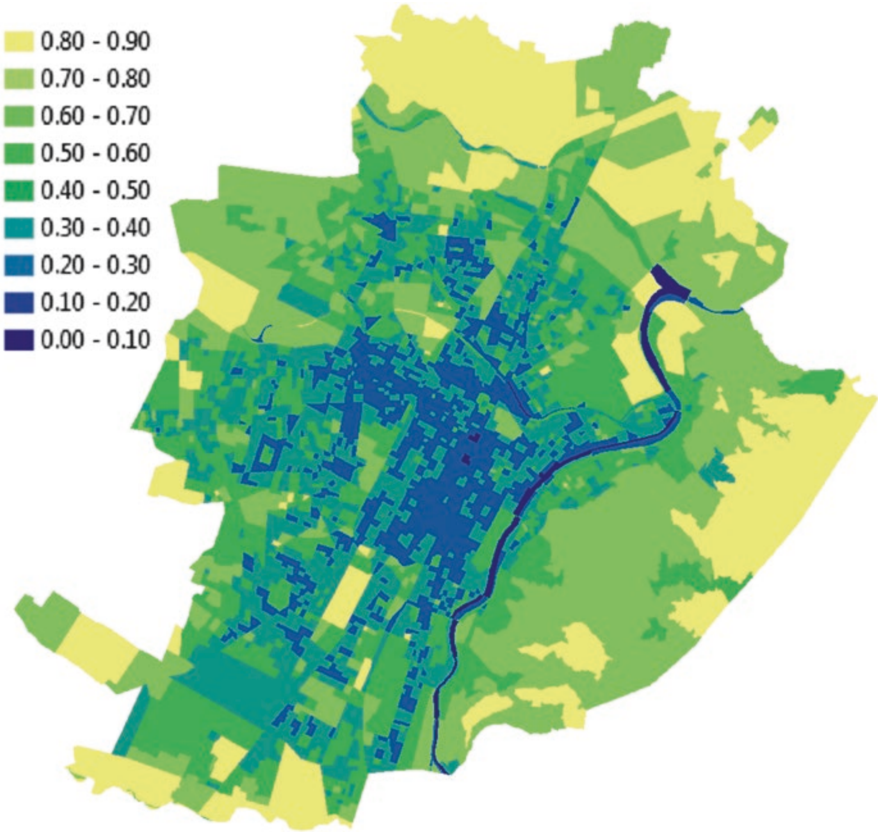

Fig. 11.8 The average value of albedo coefficient A for the census sections of Turin

Table 11.2 Characteristics of the census sections with the analysed weather stations

Turin's weather station	BCR (m^2/m^2)	BD (m^3/m^2)	H (m)	H/W (m/m)	H/H_{avg} (m/m)	MBO (−)	MOS (−)	U (−)	P (−)	A (−)
via della Consolata	0.43	7.3	17.6	0.80	1.0	1.3	1.3	0.35	1.8	0.15
Giardini Reali	0.01	0.1	13.1	0.18	1.1	1.1	1.1	0.00	1.3	0.21
Reiss Romoli	0.32	4.0	18.2	0.56	1.0	0.9	1.1	0.18	0.9	0.20
Vallere	0.14	1.0	8.4	0.58	0.8	0.8	0.8	0.08	0.5	0.20
Alenia	0.36	4.2	13.5	0.47	1.4	0.8	0.8	0.17	0.9	0.19
Buon Pastore	0.26	3.1	15.9	0.66	1.1	1.3	1.3	0.17	1.8	0.17
Italgas	0.18	1.3	9.8	0.19	0.9	1.3	1.3	0.03	1.5	0.18
Politecnico di Torino	0.39	5.8	17.9	0.54	0.9	1.3	0.8	0.21	0.9	0.17
Turin (average)	**0.34**	**4.96**	**17.85**	**0.70**	**1.0**	**1.1**	**1.05**	**0.26**	**1.17**	**0.18**

In Table 11.3, the values of the monthly air temperature registered from the weather stations are reported with the monthly air temperature gradient. This value goes from 0 to 1, and it has been calculated from the relation:

$$\Delta T_m = (T_m - T_{\min}) / (T_{\max} - T_{\min})[-] \tag{11.5}$$

and the ΔT_m will be considered uniformly distributed in the all city of Turin.

In Table 11.4 the average characteristics of the census section with the considered five weather stations are reported.

A regression analysis of the monthly air temperatures was performed considering the most influential urban variables in Eq. 11.4 to reach the measured values for each weather station in Table 11.3.

The resulting model is the following:

$$T_{air} = f(GUPA) = (22.75 \cdot \Delta T_m) + (3.31 \cdot BCR) + 0.10 \cdot H / W) + (2.38 \cdot MOS) + (0.55 \cdot H / H_{\text{aver}}) + (-0.44 \cdot A)[°C] \tag{11.6}$$

Using the model of Eq. 11.6, the air temperature is proportional with the building coverage ratio (*BCR*) (and then the building density (*BD*)), the aspect ratio (*H/W*), the main street orientation (*MOS*) and the ratio between building height and the height of the surrounding H/H_{aver}, while the air temperature is inversely proportional to the albedo coefficient *A*, as expected.

Considering the effect of the water near the weather station of Vallere, another variable can be introduced (with water, $H_2O = 1$; without water, $H_2O = 0$). Then, the resulting model is the following:

$$T_{air} = f(GUPA) = (22.76 \cdot \Delta T_m) + (2.19 \cdot BCR) + (0.99 \cdot H / W) + (2.09 \cdot MOS) + (0.74 \cdot H / H_{\text{aver}}) + (-0.56 \cdot A) + (-0.53 \cdot H_2 0)[°C]. \tag{11.7}$$

with the air temperature inversely proportional also to the presence of water, as expected.

Also the presence of vegetation was investigated, with a similar indicator as the one for the presence of water, but without better results.

As an example in Figs. 11.9 and 11.10, the results of the models (Eqs. 11.6 and 11.7) and the measured values of air temperatures are reported for the weather stations of via della Consolata and Vallere.

In Table 11.5, the relative errors of the models used are reported for all the weather stations considered. As it is possible to notice, the relative errors are under 10% with both the models considering (with Eq. 11.7) or not (with Eq. 11.6) the presence of water.

In Figs. 11.11, 11.12, 11.13, 11.14, 11.6, 11.17 and 11.18, the evaluations of the outdoor air temperatures in the city of Turin are represented with the model of Eqs. 11.6 and 11.7 as a function of the urban morphology, the solar factor, the albedo

Table 11.3 Monthly air temperatures (2005–2015) and the relative value of monthly gradients ΔT_m

Month	4	5	6	7	8	9	10	11	12	1	2	3
Via della Consolata	21.30	18.30	23.50	28.30	25.30	22.40	10.00	11.00	6.20	5.00	8.00	13.80
Giardini Reali	19.50	16.70	21.90	27.30	23.90	21.30	9.50	7.70	3.00	3.20	7.00	11.20
Reiss Romoli	20.80	17.50	23.00	27.20	24.50	21.60	9.10	9.90	5.30	3.80	7.60	12.60
Vallere	19.40	16.30	21.20	26.90	23.70	20.60	9.60	7.30	2.10	2.50	6.60	10.30
Alenia	20.50	17.30	22.50	27.10	24.10	21.10	8.90	10.60	5.30	4.00	7.10	12.80
T_m [°C]	20.30	17.22	22.42	27.36	24.30	21.40	9.42	9.30	4.38	3.70	7.26	12.14
Δ *Tm* [−]	**0.65**	**0.56**	**0.80**	**1.00**	**0.88**	**0.75**	**0.28**	**0.22**	**0.02**	**0.00**	**0.14**	**0.34**

Table 11.4 Statistical data of the census parcel with the five weather stations

	BCR (m^2/m^2)	BD (m^3/m^2)	BH (m)	H/W (m/m)	H/H_{avg} (m/m)	MBO (−)	MOS (−)	U (−)	P (−)	A (−)
Average	0.25	3.32	14.16	0.52	1.06	0.98	1.02	0.16	1.08	0.19
Standard deviation	0.17	2.86	3.97	0.22	0.22	0.22	0.22	0.13	0.49	0.02

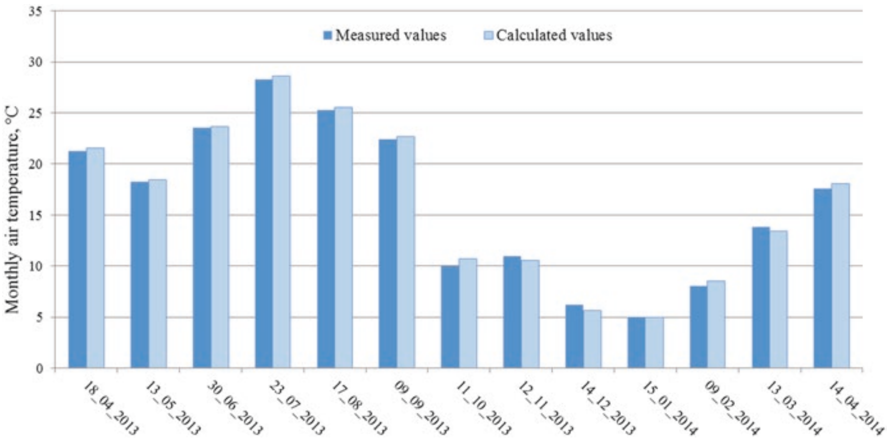

Fig. 11.9 Comparison between measured air temperatures with the weather station of via della Consolata and the calculated air temperatures as a function of $G(UPA)$ with the model (Eq. 11.6)

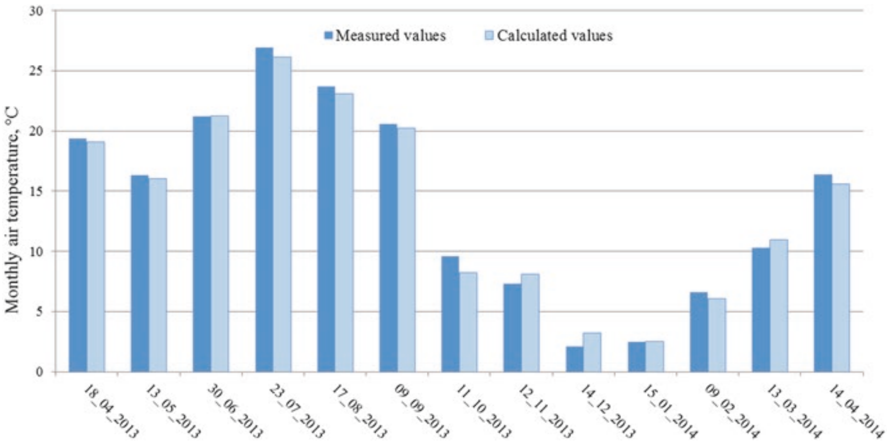

Fig. 11.10 Comparison between the measured air temperatures with the weather station of Vallere (with Po river) and the calculated air temperatures as a function of G(UPA) with the model (Eq. 11.7)

Table 11.5 The relative errors between the measured air temperatures and the calculated values with the models (Eqs. 11.6 and 11.7) for the census sections with the ARPA weather stations

Weather station	Relative error – %	
	Model Eq. 11.6	Model Eq. 11.7
Via della Consolata	3.3	3.4
Giardini Reali	4.9	4.9
Reiss Romoli	2.6	2.8
Vallere	9.5	8.2
Alenia	4.1	4.1

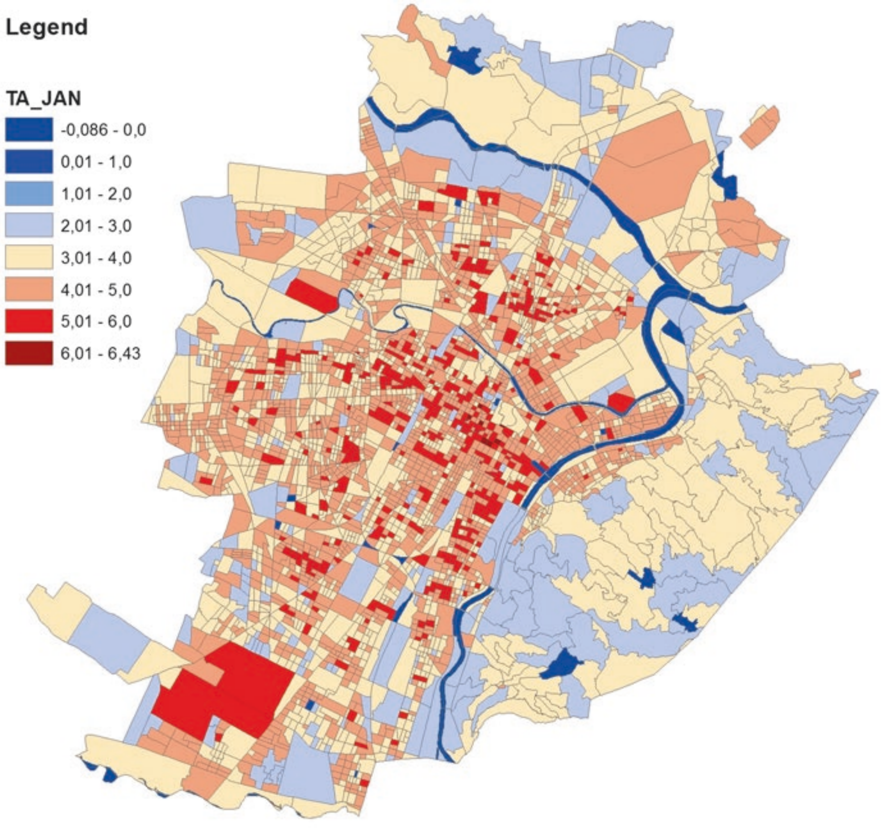

Fig. 11.11 Evaluation of outdoor air temperatures in January in the census sections of the city of Turin as a function of *G*(*UPA*) with Eq. 11.6

coefficient and the presence of water for different months during the heating and cooling seasons.

As it is possible to note, the areas near the rivers are the most cold zones with some of the areas in the hill (south-east) or near the parks. The areas near the centre

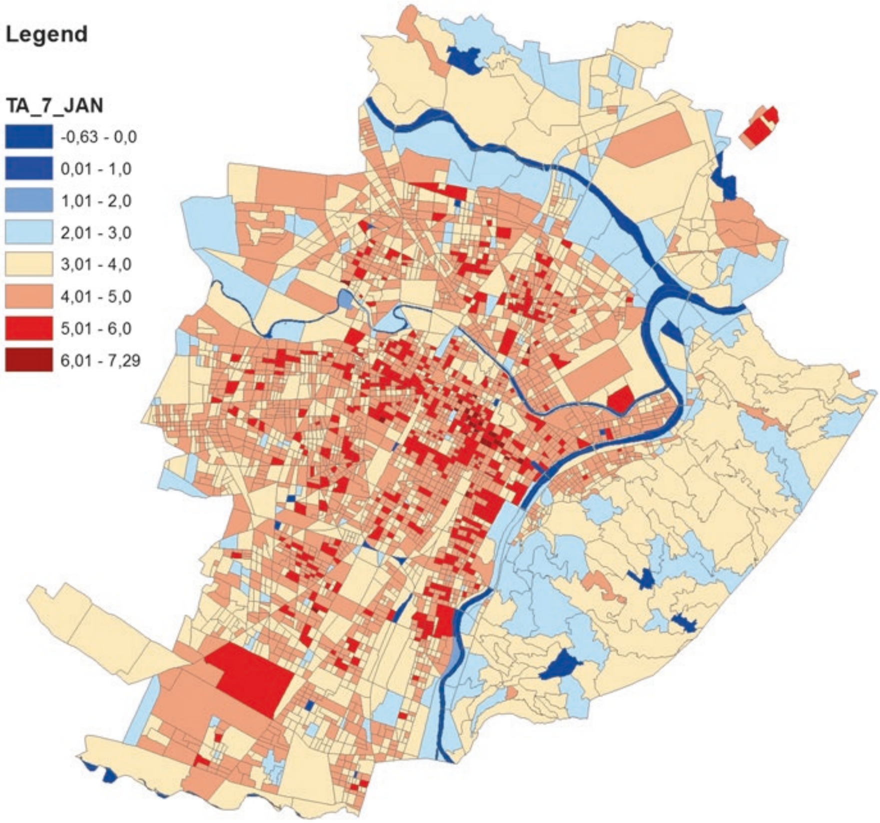

Fig. 11.12 Evaluation of outdoor air temperatures in January in the census sections of the city of Turin as a function of *G*(*UPA*) with Eq. 11.7 (considering the presence of water)

of the city with high buildings' density are the more warm together with some of the industrial zones in the southern and in the northern parts of the city. These results are confirmed in all months.

Comparing the results of the two models considering (Eq. 11.7) or not (Eq. 11.6) the presence of water in the areas, some differences can be noticed. The different influence of the aspect ratio H/W and of the presence of water must be further investigated in future works with more weather stations inside the city of Turin and comparing the results of the model with other data as the Landsat satellite images; also the presence of vegetation should be analysed.

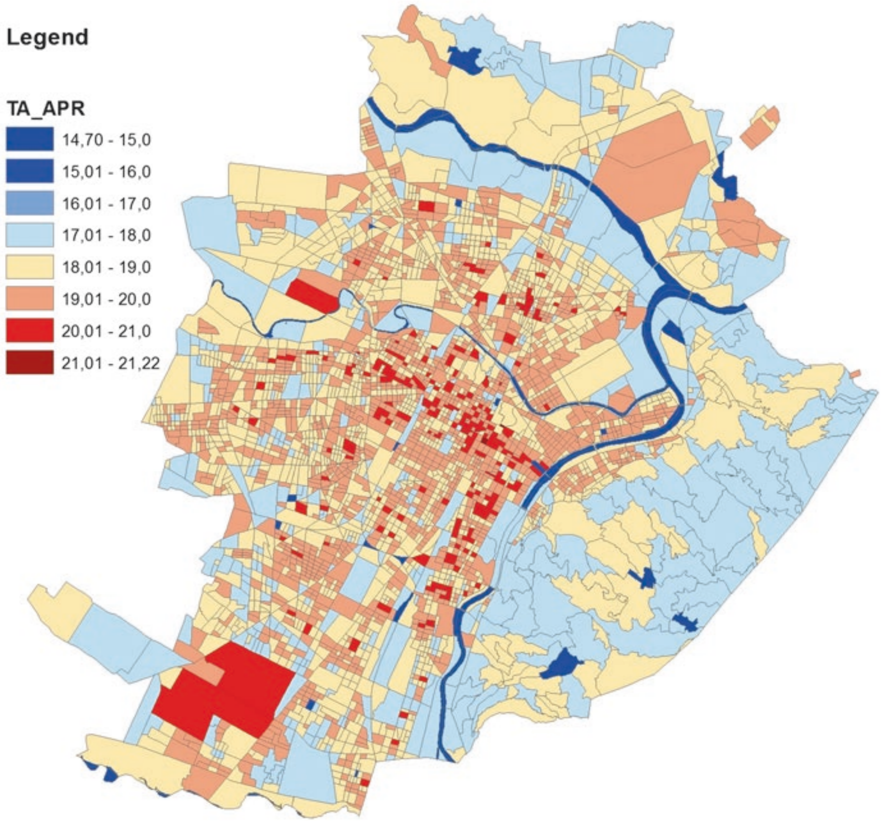

Fig. 11.13 Evaluation of outdoor air temperatures in April in the census sections of the city of Turin as a function of $G(UPA)$ with Eq. 11.6

11.6 Conclusion

In this work, the analysis of urban microclimate, the effect of urban variables and the presence of water and green surfaces have been conducted on the city of Turin, using information from the following sources: ARPA Piemonte weather stations, ASTER satellite data and urban variables from the Technical Map of the Metropolitan City of Turin.

The data acquired by weather stations are used to estimate the average monthly air temperatures measured in the areas with the weather stations in Turin; from the ASTER data, the albedo coefficient values were obtained for each point of the city and for each census sections of Turin. The Technical Map of the Metropolitan City of Turin has been used to evaluate all geometrical characteristics of the built heritage of the city of Turin to calculate the urban morphology factor U and the solar exposure P.

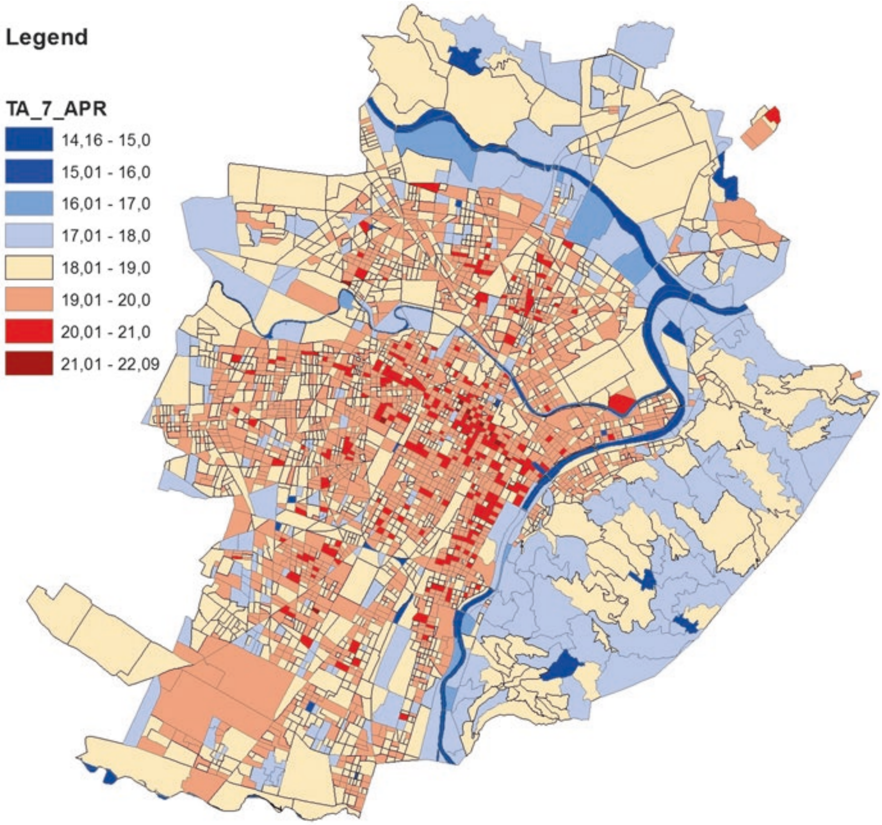

Fig. 11.14 Evaluation of outdoor air temperatures in April in the census sections of the city of Turin as a function of *G*(*UPA*) with Eq. 11.7 (considering the presence of water)

All the above information have been used to formulate two simplified models for the calculation of the outdoor air temperature: the first model calculates the air temperature taking into account the urban planning variables and the second model considering also the presence or the absence of the water.

The application of the model consents to map the air temperatures in the city of Turin for each month, according to the urban variables and the albedo coefficient of the outdoor spaces to understand the air temperature variations.

The model can be also applied in different design phases of the urban planning; it can be applied in the predesign phase to see how the project can influence the outside air temperature and then the liveability of the outdoor spaces in all the seasons. Moreover, the model can also be used to check how the different urban vari-

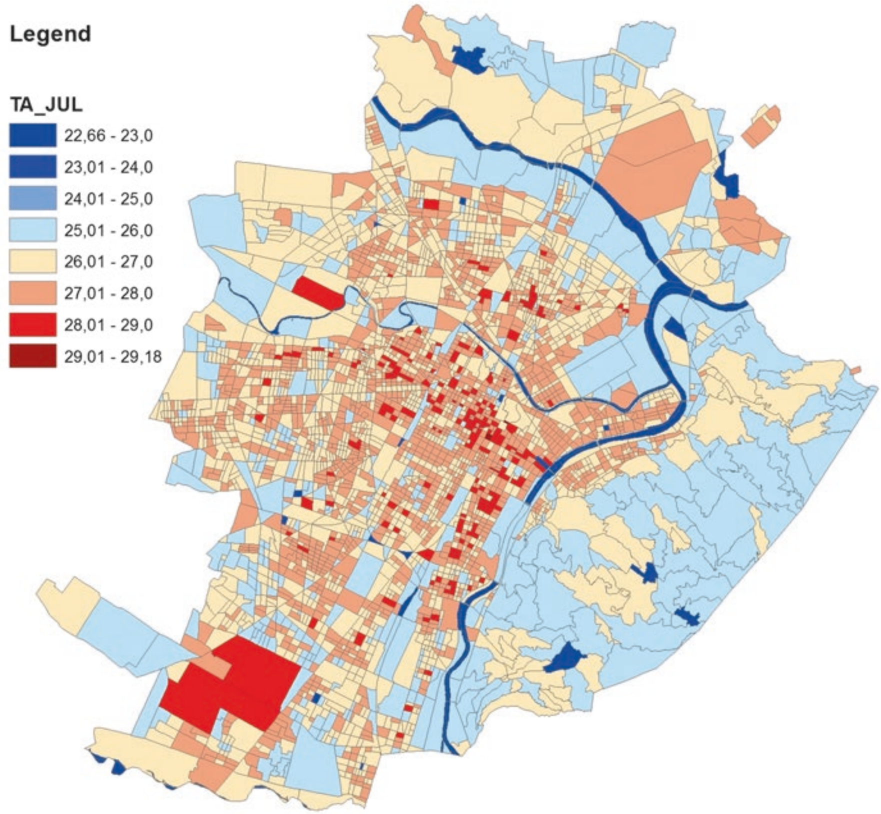

Fig. 11.15 Evaluation of outdoor air temperatures in July in the census sections of the city of Turin as a function of $G(UPA)$ with Eq. 11.6

ables can influence the outdoor air temperatures and to evaluate how to improve the liveability of the urban environment with interventions that can mitigate the microclimate at blocks of building scale.

Future works will improve the models considering more areas around Turin with weather stations and comparing also the results of the models with other satellite images as the Landsat ones.

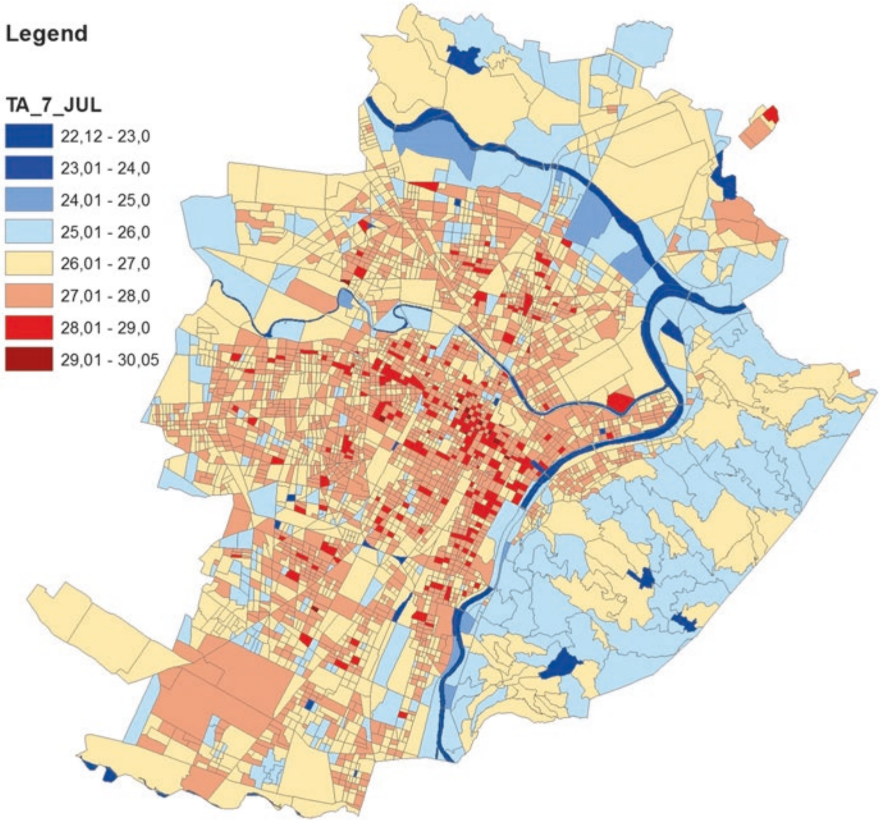

Fig. 11.16 Evaluation of outdoor air temperatures in July in the census sections of the city of as a function of *G*(*UPA*) Turin with the Eq. 11.7 (considering the presence of water)

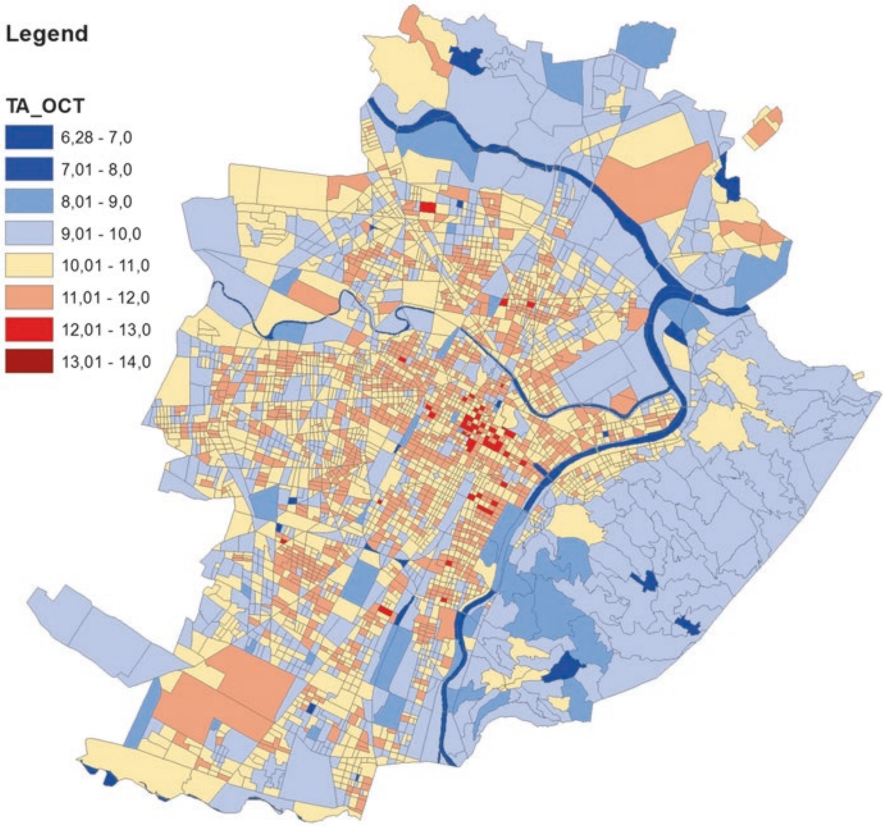

Fig. 11.17 Evaluation of outdoor air temperatures in October in the census sections of the city of Turin as a function of $G(UPA)$ with Eq. 11.6

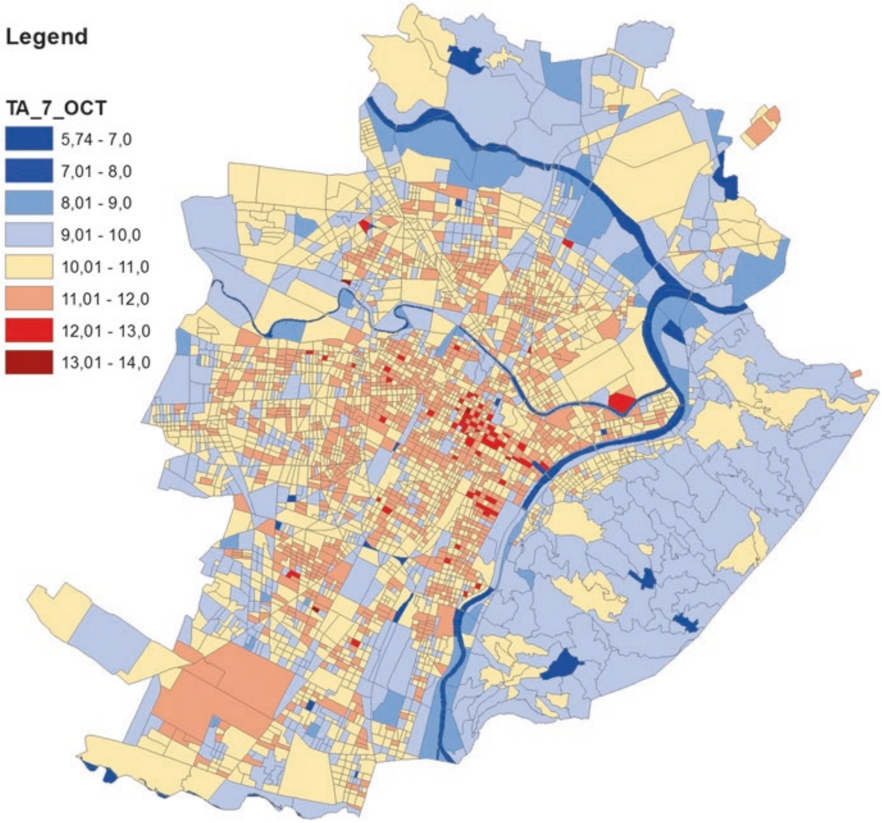

Fig. 11.18 Evaluation of outdoor air temperatures in October in the census sections of the city of Turin as a function of G(UPA) with Eq. 11.7 (considering the presence of water)

Acknowledgments A special thanks to the Master Degree students Gualtiero Ceretti, Marta Carozza, Daria Carta, José Correa Martin and Marta Repice for their support in the analysis of urban variables and in the evaluation of the albedo coefficients and finally to Chantal Diegoli (CSI Piemonte) for sharing ASTER spatial data.

References

Allegrini J et al (2014) Influence of the urban microclimate in street canyons on the energy demand for space cooling and heating of buildings. Energy and Buildings 55:823–832

Aniello C et al (1995) Mapping micro-urban heat islands using Landsat TM and a GIS. Comput Geosci 21(8):965–969

Balogun AA et al (2014) Effect of tree-shading on energy demand of two similar buildings. Energy and Buildings 81:305–315

Banerjee K, Panda S, Jain M K, Jeyaseelan A T, Sharma R Kr (2014) Comparison of aster thermal bands and feature identification using advance spectroscopic techniques. Int J Innov Sci Res 7(1):11–18
Berger T et al (2015) Impacts of climate change upon cooling and heating energy demand of office buildings in Vienna, AustriaTania. Energy and Buildings 80:517–530
Carnielo E, Zinzi M (2014) Optical and thermal characterisation of cool asphalts to mitigate urban temperatures and building cooling demand. Build Environ 60:56–65
Chun B, Guldmann J-M (2014) Spatial statistical analysis and simulation of the urban heat island in high-density central cities. Landsc Urban Plan 125:76–88
Coseo P, Larsen L (2015) Cooling the heat island in compact urban environments: the effectiveness of Chicago's Green Alley Program. Procedia Engineering 118:691–710
Dabaieh M et al (2015) Reducing cooling demands in a hot dry climate: a simulation study for non-insulated passive cool roof thermal performance in residential buildings. Energy and Buildings 89:142–152
Debbage N, Shepherd JM (2015) The urban heat island effect and city contiguity. Comput Environ Urban Syst 54:181–194
Delmastro C, Mutani G, Pastorelli M, Vicentini G (2015a) Urban morphology and energy consumption in Italian residential buildings. 4th International Conference on Renewable Energy Research and Applications ICRERA-2015, Palermo, 22–25 November 2015
Delmastro C, Mutani G, Schranz L, Vicentini G (2015b) The role of urban form and socio-economic variables for estimating the building energy savings potential at the urban scale. Int J Heat Technol 33(4):91–100
Effat HA, Hassan OAK (2014) Change detection of urban heat islands and some related parameters using multi-temporal Landsat images; a case study for Cairo city, Egypt. Urban Climate 10:171–188
Feng H et al (2014) Using land use change trajectories to quantify the effects of urbanization on urban heat island. Adv Space Res 53:463–473
Fernàndez FJ et al (2015) Optimal location of green zones in metropolitan areas to control the urban heat island. J Comput Appl Math 289:412–425
Ghulam A (2009) How to calculate reflectance and temperature using ASTER data, Center for Environmental Sciences at Saint Louis University http://www.pancroma.com/downloads/ASTER%20Temperature%20and%20Reflectance.pdf. Accessed 29 June 2016
Gracik S et al (2015) Effect of urban neighborhoods on the performance of building cooling systems. Build Environ 90:15–29
Houet T, Pigeon G (2011) Mapping urban climate zones and quantifying climate behaviors e An application on Toulouse urban area (France). Environ Pollut 159:2180–2192
Iino A, Hoyano A (1996) Development of a method to predict the heat island potential using remote sensing and GIS data. Energy and Buildings 23:199–205
Ivajnsic D, Kaligaric M, Ziberna I (2014) Geographically weighted regression of the urban heat island of a small city. Appl Geogr 53:341–353
Jusuf S K et al. (2007) The influence of land use on the urban heat island in Singapore, Habitat Int 31:232–242
Kaloustian N, Diab Y (2015) Effects of urbanization on the urban heat island in Beirut. Urban Clim 14(Part 2):154–165
Kolokotroni M et al (2014) A validated methodology for the prediction of heating and cooling energy demand for buildings within the urban heat island: case-study of London. Sol Energy 84:2246–2255
Kong F et al (2014) Effects of spatial pattern of greenspace on urban cooling in a large metropolitan area of eastern China. Landsc Urban Plan 128:35–47
Li J et al (2009) Remote sensing evaluation of urban heat island and its spatial pattern of the Shanghai metropolitan area, China. Ecol Complex 6:413–420
Li J et al (2011) Impacts of landscape structure on surface urban heat islands: a case study of Shanghai, China. Remote Sens Environ 115:3249–3263

Li Y-Y, Zhang H, Kainz W (2012) Monitoring patterns of urban heat islands of the fast-growing Shanghai metropolis, China: using time-series of Landsat TM/ETM+ data. Int J Appl Earth Obs Geoinf 19:127138

Liang S (2000) Narrowband to broadband conversions of land surface albedo I Algorithms. Remote Sens Environ 76:213–238

Liang S, Shuey CJ, Russ AL, Fang H, Chen M, Walthall C, Daughtry CST, Hunt RJ (2002) Narrowband to broadband conversions of land surface albedo: II. Validation Remote Sens Environ 84:25–41

Liu J et al (2015) Numerical evaluation of the local weather data impacts on cooling energy use of buildings in an urban area. Procedia Engineering 121:381–388

Mallick J, Rahman A, Singh CK (2013) Modeling urban heat islands in heterogeneous land surface and its correlation with impervious surface area by using night-time ASTER satellite data in highly urbanizing city, Delhi-India. Adv Space Res 52(4):639–655

Mazzotta A, Mutani G (2015) Environmental high performance urban land cover: experimentations in Urban Barriera. 6th International Building Physics Conference, Turin 14–17th June 2015, Energy Procedia, Doi:10.1016/j.egypro.2015.11.059

Merbitz H et al (2012) GIS-based identification of spatial variables enhancing heat and poor air quality in urban areas. Appl Geogr 33:94–106

Mirzaei PA (2015) Recent challenges in modeling of urban heat island. Sustainable Cities and Society 19:200–206

Misni A (2015) The effect of building construction and human factors in cooling energy use. Procedia – Soc Behav Sci 202:373–381

Morris KI et al (2015) Computational study of urban heat island of Putrajaya, Malaysia. Sustainable Cities and Society 19:359–372

Mutani G (2016) Urban planning for the liveability and thermal comfort of outdoor spaces. 11th conference on sustainable of energy, water and environmental systems, SDEWES2016.0442. Lisbon, pp 1–15, ISSN: 1847–7178

Mutani G, Gamba A, Maio S (2016) Space heating energy consumption and urban form. The case study of residential buildings in Turin (Italy). 11th conference on sustainable of energy, water and environmental systems, SDEWES2016.0441. Lisbon, pp 1–17. ISSN: 1847–7178

Onischi A et al (2010) Evaluating the potential for urban heat-island mitigation by greening parking lots. Urban For Urban Green 9:323–332

Peron F et al (2015) Urban Heat Island (UHI) mitigating strategies: a case-based comparative analysis. Sustainable Cities and Society 19:222–235

Pisello AL (2015) Thermal-energy analysis of roof cool clay tiles for application in historic buildings and cities. Sustain Cities Soc 19:271–280

Pisello AL, Cotana F (2014) The thermal effect of an innovative cool roof on residential buildings in Italy: results from two years of continuous monitoring. Energy and Buildings 69:154–164

Pisello AL, Cotana F (2015) Thermal-energy and environmental impact of cool clay tiles for residential buildings in Italy. Procedia Eng 118:530–537

Qin Y (2015) A review on the development of cool pavements to mitigate urban heat island effect. Renew Sust Energ Rev 52:445–459

Quan SJ et al (2015) A GIS-based energy balance modeling system for urban solar buildings. Energy Procedia 75:2946–2952

Raghavan K et al (2015) Influence of urban a reason environment: special reference to building materials and temperature anomalies using geospatial technology. Sustainable Cities and Society 19:349–358

Sailor DJ (2014) Risks of summertime extreme thermal conditions in buildings as a result of climate change and exacerbation of urban heat islands. Build Environ 78:81–88

Salata F et al (2015) How high albedo and traditional buildings' materials and vegetation affect the quality of urban microclimate. A case study. Energy Build 99:32–49

Santamouris M (2014a) Cooling the cities – a review of reflective and green roof mitigation technologies to fight heat island and improve comfort in urban environments. Sol Energy 103:682–703

Santamouris M (2014b) On the energy impact of urban heat island and global warming on buildings. Energy and Buildings 82:100–113

Santamouris M et al (2015) On the impact of urban heat island and global warming on the power demand and electricity consumption of buildings – a review. Energy Build 98:119–124

Schwartz N et al (2012) Relationship of land surface and air temperatures and its implications for quantifying urban heat island indicators – an application for the city of Leipzig (Germany). Ecol Indic 18:693–704

Shahidan MF et al (2015) An evaluation of outdoor and building environment cooling achieved through combination modification of trees with ground materials. Build Environ 58:245–257

Stathopoulou M, Cartalis C (2009) Downscaling AVHRR land surface temperatures for improved surface urban heat island intensity estimation. Remote Sens Environ 113:2592–2605

Theophilou MK, Serghiedes D (2015) Estimating the characteristics of the Urban Heat Island effect in Nicosia, Cyprus, using multiyear urban and rural climatic data and analysis. Energy Build 108:137–144, 157

Touchaei AG, Wang Y (2015) Characterizing urban heat island in Montreal (Canada) – effect of urban morphology. Sustain Cities Soc 19:395–402

Unger J et al (2010) Comparison and generalisation of spatial patterns of the urban heat island based on normalized values. Phys Chem Earth 35:107–114

United Nations (2014) World Urbanization Prospects: the 2014 Revision, Highlights (ST/ESA/SER.A/352). Department of Economic and Social Affairs, Population Division, ISBN 978-92-1-123195-3

Weng Q, Lung D, Schubring J (2004) Estimation of land surface temperature–vegetation abundance relationship for urban heat island studies. Remote Sens Environ 89:467–483

Xu LY, Xie XD, Li S (2013) Correlation analysis of the urban heat island effect and the spatial and temporal distribution of atmospheric particulates using TM images in Beijing. Environ Pollut 178:102–114

Yang J, Wang ZH, Kaloush KE (2015) Environmental impacts of reflective materials: is high albedo a ‘silver bullet’ for mitigating urban heat island? Renew Sust Energ Rev 47:830–843

Yeo IA, Yoon SH, Yee JJ (2013) Development of an Environment and energy Geographical Information System (E-GIS) construction model to support environmentally friendly urban planning. Appl Energy 104:723–739

Zhang Y et al (2012) Study on urban heat island effect based on normalized difference vegetated index: a case study of Wuhan City. Procedia Environ Sci 13:574–581

Zhang H et al (2013) Analysis of land use/land cover change, population shift, and their effects on spatiotemporal patterns of urban heat islands in metropolitan Shanghai, China. Appl Geogr 44:121–133

Zhang B et al (2014) The cooling effect of urban green spaces as a contribution to energy-saving and emission-reduction: a case study in Beijing, China. Build Environ 76:37–43